applied sciences

MDPI

Article

Switchable Fiber Ring Laser Sensor for Air Pressure Based on Mach–Zehnder Interferometer

Adalberto Perez-Guzman [1], Julian M. Estudillo-Ayala [1,*], Daniel Jauregui-Vazquez [2], Juan C. Hernandez-Garcia [1,3], Javier A. Martin-Vela [4], Tania Lozano-Hernandez [1], Jose D. Filoteo-Razo [5], Juan M. Sierra-Hernandez [1] and Roberto Rojas-Laguna [1]

[1] Departamento de Ingeniería Electrónica, División de Ingenierías Campus Irapuato Salamanca, Universidad de Guanajuato, Carretera Salamanca-Valle de Santiago km 3.5 + 1.8 km, Salamanca 36885, Mexico; a.perezguzman@ugto.mx (A.P.-G.); jchernandez@ugto.mx (J.C.H.-G.); t.lozanohernandez@ugto.mx (T.L.-H.); jm.sierra@ugto.mx (J.M.S.-H.); rlaguna@ugto.mx (R.R.-L.)
[2] Centro de Investigación Científica y de Educación Superior de Ensenada (CICESE), División de Física Aplicada-Departamento de Óptica, Carretera Ensenada-Tijuana, No. 3918, Zona Playitas, Ensenada 22860, Mexico; djauregui@cicese.mx
[3] Investigadoras e Investigadores por Mexico CONAHCYT, Consejo Nacional de Humanidades Ciencias y Tecnologías, Av. Insurgentes Sur 1582, Col. Crédito Constructor, Benito Juárez 03940, Mexico
[4] Tecnologíco Nacional de México Campus Conkal, Avenida Tecnológico s/n Conkal, Mérida 97345, Mexico; javier.martin.vela@gmail.com
[5] Facultad de Ingenieria y Ciencias, Universidad Autonoma de Tamaulipas, Ciudad Victoria 87149, Mexico; darazo@uat.edu.mx
* Correspondence: julian@ugto.mx

Abstract: This work shows a study of pressure gas sensing using an optical fiber interferometer inside a gas cell; here, a thin-core fiber modal interferometer (TCFMI) is fabricated using two distinct types of fiber, a single-mode fiber (SMF model 1060XP) and thin-core fiber (TCF model 460 HP). This interferometric structure is set into a ring fiber laser with an ytterbium-doped fiber (YDF) pumped with a 980 nm laser diode. The TCFMI interference spectrum shows wavelength shifting and amplitude variations as the chamber pressure is altered in the range of 5 to 40 PSI; these changes control the ring fiber laser cavity response linearly and lead to good stability in its wavelength operation in a range of 30 nm. The proposed interferometer operates as a wavelength-selective filter in the fiber ring laser cavity. The single laser emission shows a side mode suppression ratio of 34.17 dB. The fiber ring laser is a reliable alternative for air pressure sensing applications.

Keywords: Mach–Zehnder interferometer; ytterbium; ring lasers; fiber optic sensors

check for updates

Citation: Perez-Guzman, A.; Estudillo-Ayala, J.M.; Jauregui-Vazquez, D.; Hernandez-Garcia, J.C.; Martin-Vela, J.A.; Lozano-Hernandez, T.; Filoteo-Razo, J.D.; Sierra-Hernandez, J.M.; Rojas-Laguna, R. Switchable Fiber Ring Laser Sensor for Air Pressure Based on Mach–Zehnder Interferometer. *Appl. Sci.* **2023**, *13*, 12607. https://doi.org/10.3390/app132312607

Received: 19 October 2023
Revised: 14 November 2023
Accepted: 20 November 2023
Published: 23 November 2023

Copyright: © 2023 by the authors. Licensee MDPI, Basel, Switzerland. This article is an open access article distributed under the terms and conditions of the Creative Commons Attribution (CC BY) license (https://creativecommons.org/licenses/by/4.0/).

1. Introduction

Fiber-based devices have become essential in implementing sensor technologies, lasers, and communications because of their sensing capability in unfavorable environments, immunity to electromagnetic fields, and compactness. Fiber optic sensors have been emerging as a desirable device for the measurement of a wide variety of physical and chemical parameters in different environments, including the measurement of temperature [1–3], pressure [1], strain [4], curvature [3], displacement [5], pH values [6], humidity [7], and refractive index [8]. Optical fiber pressure sensors are of significant interest due to their compact size and signal detection. In them, different properties of the transmitted light can be modified to carry information about the measured variable. These sensors employ various mechanisms that have been reported, including micro-bending [9] and fiber gratings sensors [3,10], Fabry–Perot interferometers [11–14], tapered long-period grating [15], lossy mode resonances [16] and Mach–Zehnder interferometers [17–20]. These published works are mainly in the research phase. They use different sensing techniques and improve the experimental setups to make all-fiber configurations.

Several fabrication techniques have been proposed to construct the in-line Mach–Zehnder interferometer, including the SMF-MMF-SMF structure [21–24], multimode fiber–polarization-maintaining fiber Bragg grating–multimode fiber (MMF-PMFBG-MMF) [25], core offset [26], fiber tapering [27], photonic crystal fiber (PCF) configurations [28], twin-core fiber [29] and thin-core fiber modal interferometers [30–39], and cascade fiber MZIs [40], among others. The sensor proposed by Yujia Zhao, cascaded fiber MZIs, for simultaneous measurement of pressure and temperature, which consists of the cascade the splicing of two MZIs, gives an overview of the implementation of different types of fibers for the creation of the MZI, as well as tapers.

The idea of operating with a modal interferometer using two types of fibers, differentiated by the diameter of their core, resulted in the TCFMI. This work differs from the one proposed by Yizheng Zhu, and presents a miniature fiber optic pressure sensor made from a Fabry–Perot cavity and a thin silica membrane fabricated via techniques involving fusion splicing and wet chemical etching, using a microscope to make the device splices, and seeks to make a small but more straightforward device to fabricate and manipulate that is low cost using a small length of thin-core fiber. In the literature, thin-core fibers have been employed for temperature [1,30,31], curvature [32,33], refractive index [34], strain [30], gas pressure [35], liquid level [36], pH values [37], humidity [38], and ammonia gas [39]. Y. Liu et al. demonstrated a gas pressure sensor based on a twisted off-axis double strain and an air gap induced by a femtosecond laser in a commercial single-mode fiber (SMF), achieving a phase shift in the interferometer cladding arm. Z. Li et al. proposed a Mach–Zehnder interferometer based on a twin-core fiber splicing a short section of dual-core fiber between two single-mode fibers. A microchannel was created to form an interferometer arm using a femtosecond laser to pierce one core of the dual-core fiber. In contrast, the core of the other fiber functioned as a reference arm. A gas pressure sensor based on a TCFMI has not been reported in the literature, having as advantages the dimension of the configuration, a pressure range of 45 PSI, and the capability of implementation as a sensor and as a switchable fiber ring laser sensor with a selection of focus areas.

Another experimental work presents a robust optical fiber modal Mach–Zehnder (MZ) interferometer, which is embedded in a fiber ring laser system, as a tunable filter to improve the detection limit (DL) due to its narrow full-width at half-maximum (FWHM) and high signal-to-noise ratio (SNR) [41]. The principal difference is based on the sensing element, comprising two cascaded up-taper joints fabricated via shoving fusion. Likewise, there are works in which the authors use fiber ring laser demodulation technology [42]. Alternatively, some papers propose a fiber laser sensor based on a ring cavity configuration. The cavity is operated by a core-offset Mach–Zehnder interferometer, which is used as a wave selection filter and temperature detection device. Here, the proposed fiber laser sensor exhibits sensing properties, such as a sensitivity of 0.03119 pm/°C, a dynamic range of 90 °C, and a signal-to-noise ratio of 52 dB [43], as well as a highly stable and switchable dual-wavelength laser using a coupled microfiber Mach–Zehnder interferometer as an optical filter [44]. Moreover, ring fiber laser sensors have been employed to measure various parameters. These include gas pressure using a Fabry–Perot interferometer and a Sagnac Interferometer [45], temperature measurements utilizing fiber Bragg gratings (FBG) [46], gas concentration sensing based on a hollow-core photonic crystal fiber [47], and distributed pressure sensing employing a mode-locked laser [48].

Based on comparisons with previous research described in the Introduction section, we present a switchable fiber ring laser sensor for air pressure using an MZI, where the MZI implemented is made with a section of thin-core optical fiber spliced between two sections of standard single-mode fiber, using as a broad spectrum light source the amplification spontaneous emission (ASE) of an ytterbium-doped fiber pumped with a 980 nm laser diode, and obtaining an emission spectrum of 1020 to 1200 nm; this range of wavelengths helped us to characterize our interferometer observing the interference fringes. A ring laser was implemented in the region close to one micron of operation; inside the loop, the Mach–Zehnder interferometer was added and fixed inside the gas cell, thus achieving an

air pressure laser sensor. This laser sensor obtained relevant results by varying the air pressure inside the cell, obtaining different emissions of wavelengths. The basic principle of operation of our sensor is that by introducing the interferometer inside the cell and applying air inside it, the interferometer undergoes stress due to pressure; this stress causes the refractive index of the interferometer fiber to change. The power spectrum responds to fluctuations in air pressure, and the device can measure within a range of 5 to 40 PSI while maintaining wavelength stability. Finally, this paper's novelty is based on investigating pressure gas sensing using a thin-core fiber modal interferometer (TCFMI) composed of a single-mode fiber and a thin-core fiber. Integrated into an ytterbium-doped fiber (YDF) ring fiber laser, it responds effectively to chamber pressure changes, controlling the laser cavity response with wavelength shifts and amplitude variations. The interferometer also functions as a wavelength-selective filter, achieving a remarkable side mode suppression ratio (SMSR) of 34.17 dB.

2. Principle of Operation and Its TCFMI Pressure Analysis

The TCFMI was fabricated using a segment of TCF with a small core diameter spliced between two SMFs. The SMF sections of Nufern 1060-XP (East Granby, CT, USA), with a core diameter of 5.8 µm for wavelengths ranging from 980–1600 nm, were employed. Meanwhile, the model of a segment of TCF is Nufern 460-HP; it has a core diameter of 2.5 µm and operates from 450 nm to 600 nm. It was manufactured via fusion splicing using an FSM-100M (Singapore) Fujikura splicer. Table 1 shows the main parameters of the fibers used to produce the TCFMI.

Table 1. 1060-XP and 460-HP fiber parameters.

Items	SMF	TCF
Core diameter (µm)	5.8	2.5
Cladding diameter (µm)	125	125
Refractive index of core	1.4512	1.4505
Refractive index of cladding	1.447	1.447

Figure 1 shows the segment of TCF(460-HP) in the middle section of the interferometer has a small length of L = 8.5 cm, which was used to obtain minimal insertion losses in the interference pattern, approximately −11 dB, and reaching a depth in the fringes of −20 to −25 dB. Figure 2 shows the spectrum signal generated by the proposed TCFMI. The main principle of the proposed TCFMI can be explained by considering the general theory of the operation of the modal interferometer principle. Equation (1) determines the spectrum response:

$$I = I_1 + I_2 + 2\sqrt{I_1 I_2}cos\left[\frac{2\pi\left(n_{eff}^{co} - n_{eff}^{cl}\right)}{\lambda}L\right] \quad (1)$$

where I_1 and I_2 are the intensities of the core and cladding, respectively, of the Nufern 460-HP fiber, λ is the free space wavelength of the light fiber material, L is the length of the segment of TCF, and finally, n_{eff}^{co} and n_{eff}^{cl} represent the effective refractive index involved.

When the fundamental mode propagates through the first section of the Nufern 1060-XP fiber until it reaches the first interface of the TCMFI, high-order cladding modes are generated in the Nufern 460-HP fiber due to the misalignment of the core of the fibers involved in this. Upon reaching the second interface, part of these modes are recoupled to the Nufern 1060-XP fiber core, and the excited fiber cladding modes interfere with the core mode, forming some local maximum or minimum interference points, respectively. By

considering a local minimum at the endpoint, i.e., a transmit dip in the transmit spectrum, the relative phase shift of the two interfering modes can be described as:

$$2\pi\left(n_{eff}^{co} - n_{eff}^{cl}\right)\frac{L}{\lambda_D} = (2k+1)\pi \tag{2}$$

Here, k is an integer; then, the intensity of interference light reaches a minimum, corresponding to the wavelength as follows [41]:

$$\lambda_D = \frac{2\left(n_{eff}^{co} - n_{eff}^{cl}\right)L}{(2k+1)} \tag{3}$$

Equation (3) shows that either the effective refractive index or length differences can affect the fringe pattern or both changes. In our case, these parameters were controlled when the TCFMI interacted with the pressure inside the gas cell.

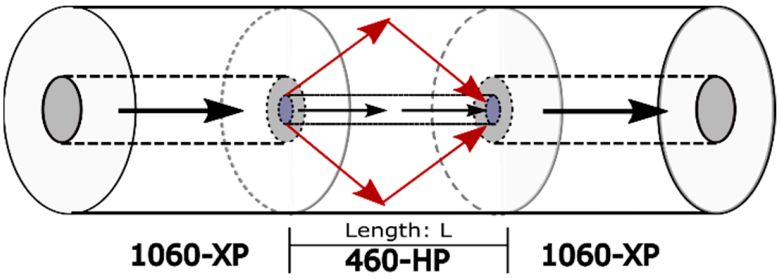

Figure 1. TCFMI schematic diagram.

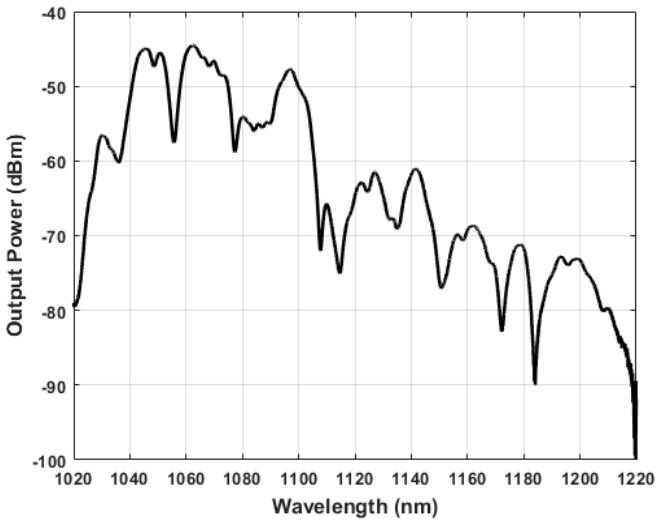

Figure 2. Optical spectrum of the TCFMI.

The scheme in Figure 3 was implemented to study the pressure response of the TCFMI. This setup employed a QPHOTONICS QDFBLD-980-350 (Ann Arbor, MI, USA) semiconductor laser diode inside a Thorlabs CLD1015 controller as our pump source, followed by a WDM, which is a wave division multiplexer; as an active medium, we used ytterbium-doped fiber (Thorlabs YB1200, Newton, NJ, USA), with a length of 2.8 m, a core diameter close to 10 µm, and a high concentration of nearly 9×10^{19} ions/cm^{-3}, which worked at the same wavelength as the pumping source. Afterward, a polarization controller was set to manipulate the polarization stage; moreover, an optical fiber isolator

was used to avoid feedback from the system; between these elements, 120 m of 1064 nm single-mode fiber was set. Finally, the gas cell contained the interferometer interacting with the pressure inside it, thus changing the output interference pattern; the fiber laser system response was analyzed and visualized using an optical spectrum analyzer (OSA), YOKOGAWA AQ6370B (Tokyo, Japan). This setup was the base of the pressure ring fiber laser cavity.

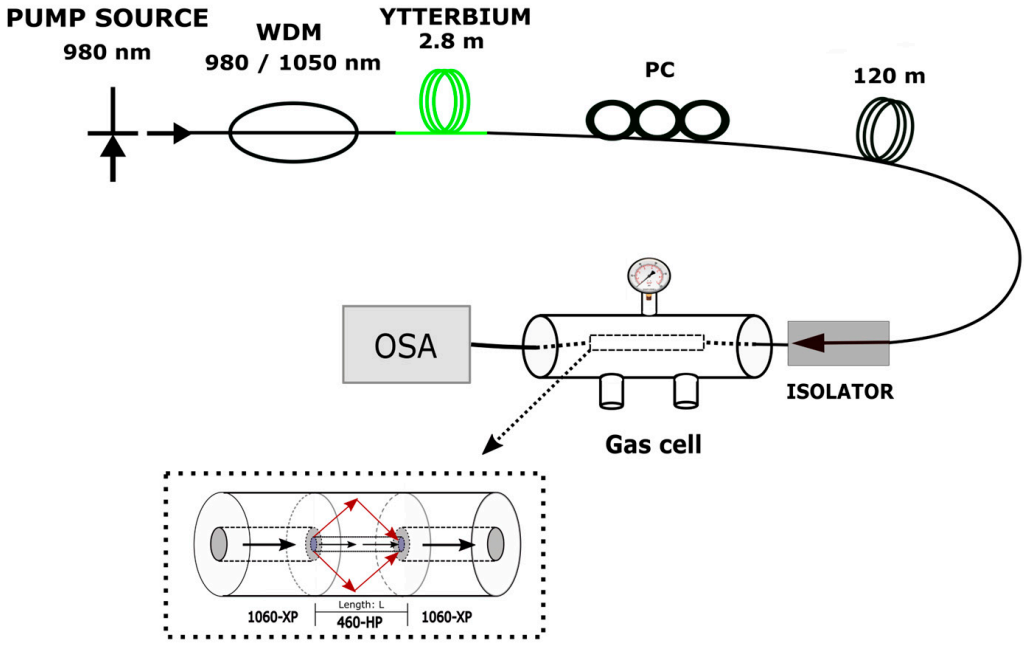

Figure 3. Experimental setup to characterize the TCFMI as its surrounding pressure was modified.

The gas cell was made using a metal tube with two gas inlet taps and an analogous manometer in the upper part of the tube from which the information on the pressure inside the cell was collected. At the ends are two metal covers with thick glass and a small hole in the center of this where the optical fiber passed through. Air was introduced to the cell using a small air compressor to put pressure on the interferometer, and thus, obtain the interference patterns according to the pressure change inside it, which ranged from 0 to 40 PSI. Figure 2 shows the interference transmission spectrum as the ASE spectrum was generated. An air compressor controls the pressure inside the chamber; the interference pattern is altered as the pressure changes. Figure 4 shows power and wavelength variations as the air pressure increases. Here, several regions display linear power decrements. The measurements were made in a range from 0 to 40 PSI, using a 5 PSI resolution. The interference pattern shifted toward longer wavelengths as indicated by the direction of the red arrows in Figure 4b, as a result, the wavelength peak changed from 1074 to 1080 nm, as shown (see Figure 4b).

Figure 5 represents the change in wavelength of the signal obtained from the ASE noise of the ytterbium-doped fiber by increasing the pressure inside the cell where the TCMFI is located. The graph in Figure 4b was obtained with a constant power output (approx. −50 dBm) for pressure values of 0, 5, 10, 20, 25, 30, and 40 PSI; an approximate redshift of 3.5 nm is observed from the minimum to the maximum air pressure. As a result, the TCMFI exhibits a sensitivity of 0.0925 nm/PSI in the 0–40 PSI range.

(**a**)

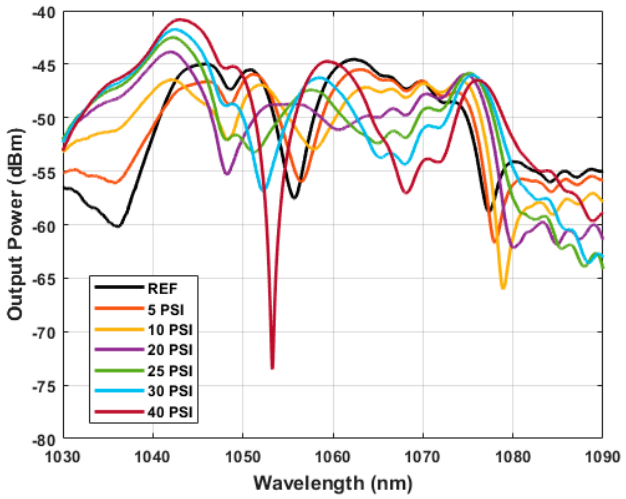

(**b**)

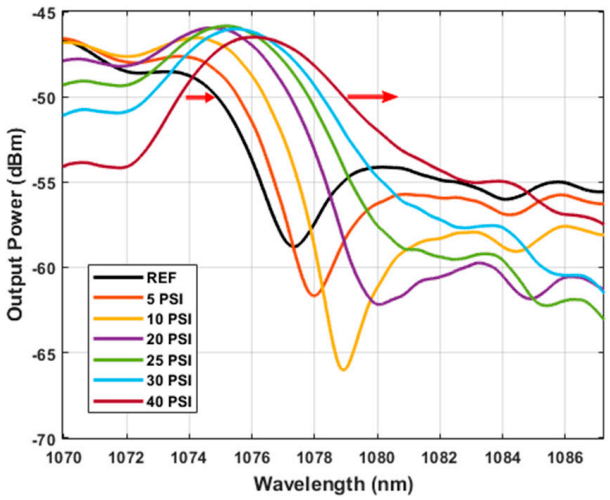

Figure 4. (**a**) Spectrum for different air pressure values and (**b**) spectrum for different air pressure values in the range from 0 to 40 PSI.

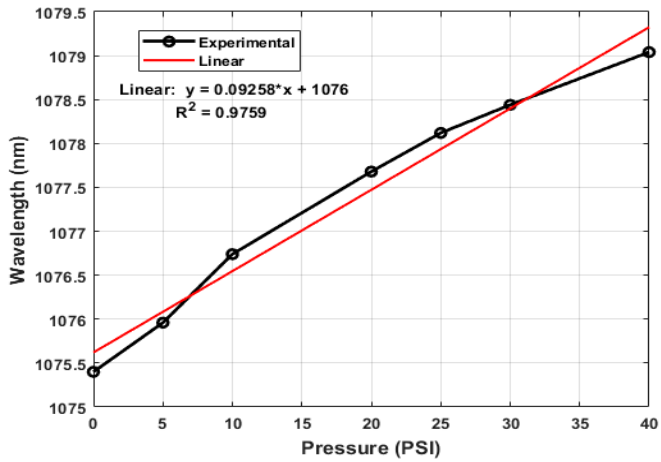

Figure 5. Graph of the displacement of the wavelength with increasing air pressure in signal of ASE of YDF.

3. Results and Discussion

Based on the conventional ring fiber laser cavity, as shown in Figure 6, the elements described in Figure 3 were closed to form a ring cavity by a 90/10 optical fiber coupler, allowing us to return 90% of the signal to the system as feedback. This cavity length increment provided a flat spectrum of 1060 to 1120 nm [27].

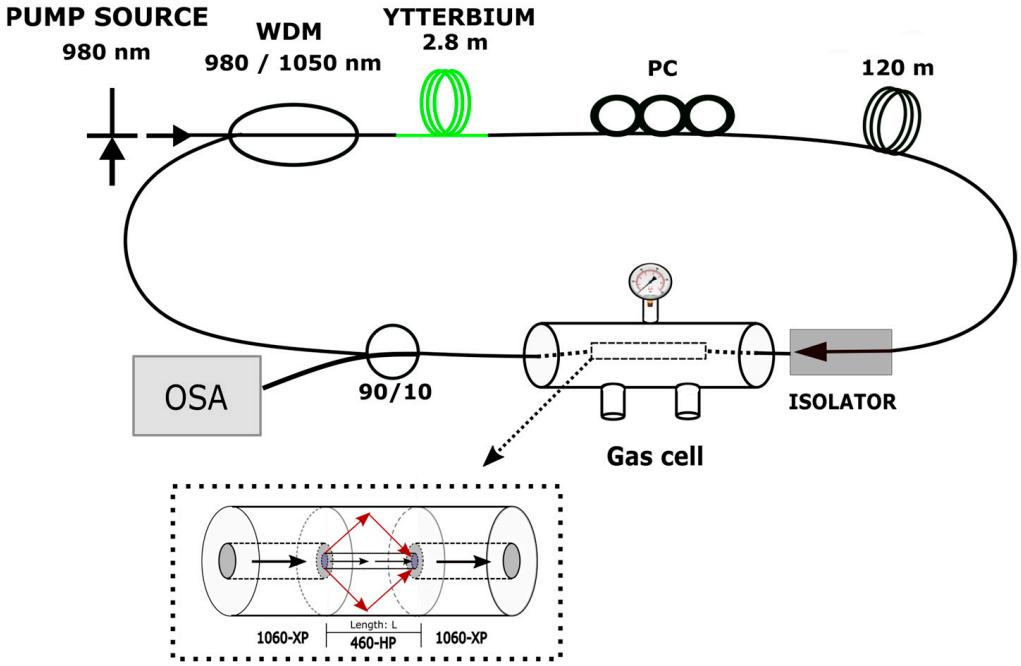

Figure 6. Experimental setup of the fiber laser.

The response of the laser is demonstrated in Figure 7. A single-line emission was generated at 1063.04 nm for the initial conditions with a side mode suppression ratio (SMSR) of 34.17 dB. These results of emissions, as well as all the results shown in the manuscript, were recorded using an OSA resolution of 0.2 nm.

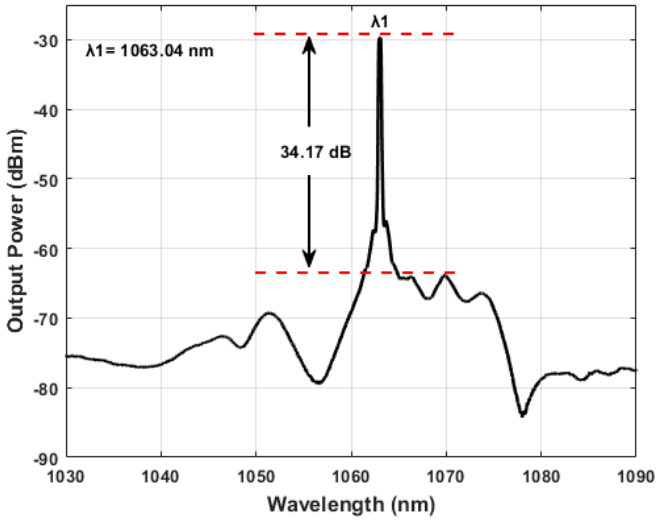

Figure 7. Reference laser emission.

Figure 8 shows that when the pressure inside the gas cell increases, the laser emission shifts to the right of the reference until it reaches 25 PSI, and then, switches to the other side at 30 and 40 PSI.

The result shows that by increasing the air pressure inside the cell, the TCFMI undergoes stress. The modes inside of the TCFMI are affected by changes in the refractive index due to the photoelastic effect. It is essential to note that the fiber laser is switchable. Table 2 shows the wavelength of the laser emission peaks as the air cell pressure increases from 0 to 40 PSI.

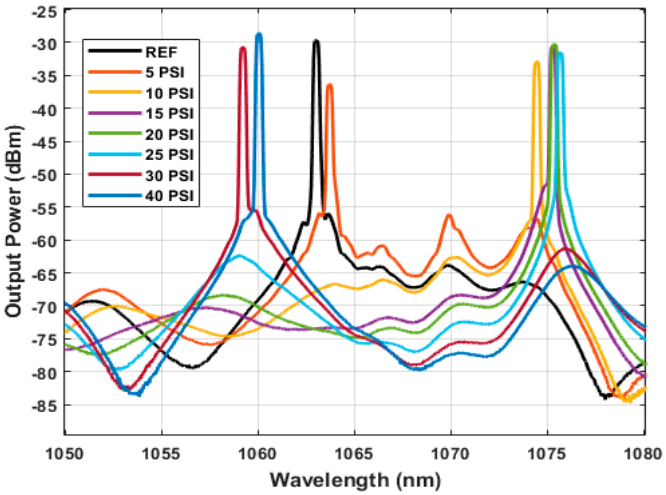

Figure 8. Laser emission spectra for different pressure values.

Table 2. Wavelength of laser emissions.

REF	λ1 = 1063.04 nm
5 PSI	λ2 = 1063.72 nm
10 PSI	λ3 = 1074.48 nm
15 PSI	λ4 = 1075.28 nm
20 PSI	λ5 = 1075.40 nm
25 PSI	λ6 = 1075.68 nm
30 PSI	λ7 = 1059.20 nm
40 PSI	λ8 = 1060.04 nm

As shown in Figure 9, a switchable fiber laser response is observed within a specific range. In the area delimited in blue, as the pressure increases from 0 to 5 PSI, it shifts 0.68 nm upon reaching 10 PSI; in the region of red color, represented in Figure 10, the relationship between the pressure and the laser wavelength presents a certain linearity. As the pressure increases, the wavelength of the laser emission shifts toward wavelengths in the red region. A sensitivity of 0.0744 nm/PSI in the range of 10–25 PSI with a step of 5 PSI is achieved for the laser. The switching occurs at a pressure of 30 PSI, as seen in the green region.

Maintaining a constant pressure of 30 PSI inside the cell, the output spectrum was scanned for 30 min and recorded after 5 min intervals (see Figure 11a) with a resolution of 0.2 nm. This experimentation was conducted at ambient room temperature to confirm the laser's operational stability. Furthermore, it allowed for the examination of alterations in laser emissions when transitioning pressure between 25 and 30 PSI, and vice versa, over 30 min. Notably, it was observed that the laser emission reverted to 1075.68 nm (as shown in Figure 11b).

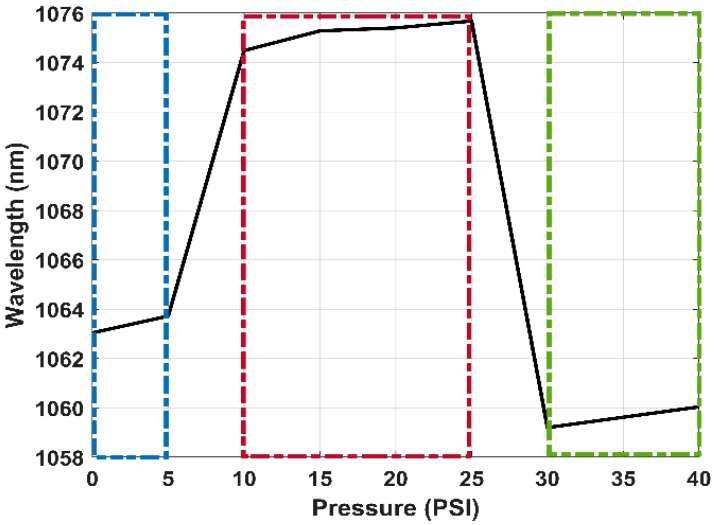

Figure 9. Response of the shift in the wavelength in the laser ring configuration when the pressure is increased in the gas cell where the TCFMI is.

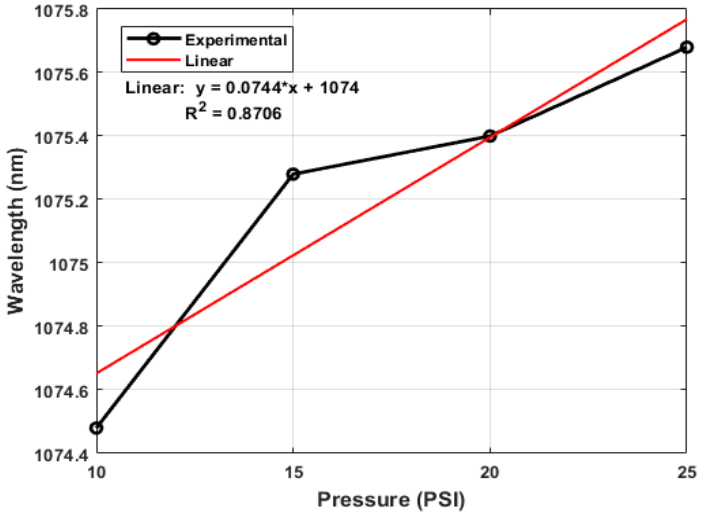

Figure 10. Zoomed-in view of the red area of Figure 9 in response of the shift in the wavelength.

The sensitivities achieved were compared with prior MZI optical fiber structures in Table 3. The sensitivity of the proposed sensor is satisfactory, like those reported in other works of air-channel-based structures. However, the proposed sensor has a simple fabrication process and high resolution.

Table 3. Sensitivity of pressure sensor for MZI structure.

Pressure Sensor	Sensitivity
This work—TCFMI	0.0925 nm/PSI ≈ 13.23 nm/MPa
Twin-core fiber with a micro-channel in one core [29]	−9.6 nm/MPa
An MZI based on core-cladding interference with a pair of off-axis twisted distortion points [35]	−5.183 nm/MPa
Cascaded fiber MZIs for simultaneous measurement of pressure [40]	78.553 nm/MPa
MZI with a micro-channel across the fiber core [49]	~8.239 nm/MPa

(**a**)

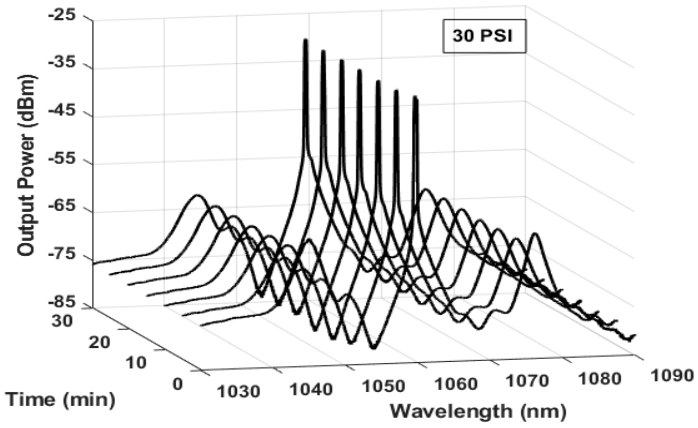

(**b**)

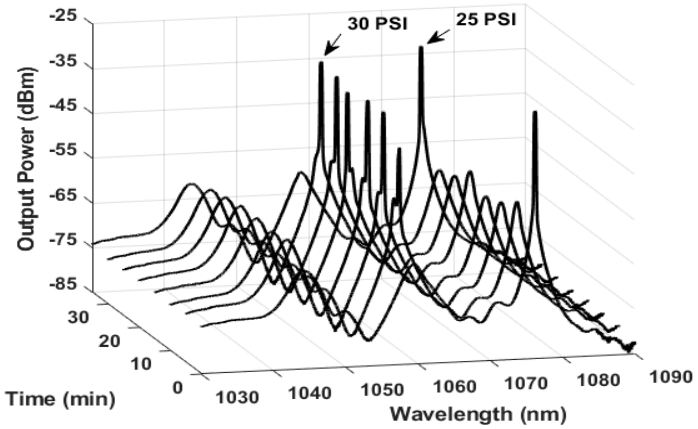

Figure 11. (**a**) Measurement of laser emission stability at 30 PSI recorded every 5 min and (**b**) Laser emission spectrum when varying the cell pressure from 25 to 30 PSI.

It needs to be emphasized that the 120 m fiber reel generated power losses. Although this power decreases, extending the laser sensor dynamic range is possible because the gain (G) is locked to the ring cavity losses (βring); therefore, if these losses are small, the gain will be equal. Moreover, the high feedback power at the YDF (P_s^{in}), caused by the low cavity loss, intensely saturated the YDF gain [43]. Then, according to Figure 4b, G and βring are altered by the TCMFI in the ring fiber sensor cavity when pressure is applied. As a result, the change alters the wavelength emissions of the laser output.

To characterize the fiber laser within the ring configuration, we employed the Mach–Zehnder optical filter, which exhibited optimal performance prior to any pressure variations. With this setup, we achieved a well-defined Gaussian profile centered at λ = 1063.04 nm and with a side mode suppression ratio of 34.17 dB. With a maximum pressure of 25 PSI for the switching action on the right side of the spectrum, we have 0 to 25 PSI, and on the left side, we have 25 to 40 PSI. These results are presented in Figure 8. Finally, it is necessary to mention the suitable stability obtained in the laser emission, as shown in Figure 11, in addition to the excellent repeatability in laser switching.

4. Conclusions

The proposed optical fiber pressure sensor can be applied to different gases, where air was used for the tests, obtaining excellent results given the changes in the interference fringes generated by the interferometer as the pressure increased and presenting good stability in its wavelength. As can be seen in the results, there is a change in the interference

patterns caused by the pressure inside the gas cell that goes from 5 PSI to 40 PSI; this part is classified as the sensing part, since the wavelength of each band is unique in each measurement, when the sensor is in operation. We can see one of these bands in our monitoring system; we will be able to know the pressure in the cell. We observe how the fringes move due to the pressure in the interferometer, causing it to change its structure and making us see a shift in the wavelength of the spectrum. Another notable advantage of this sensor lies in its sensitivity, attributed to its wide dynamic range and higher resolution compared to other sensors. The potential applications of this laser technology encompass a wide array of fields, including microfluidics, medicine, bionics, robotics, and aerospace, where changes may be challenging to detect, and the use of electronic devices is impractical due to confined spaces and electromagnetic interference.

Author Contributions: Conceptualization, J.M.E.-A., D.J.-V. and J.C.H.-G.; methodology, J.M.E.-A., J.M.S.-H. and R.R.-L.; investigation, J.M.E.-A., A.P.-G. and J.A.M.-V.; writing—original draft preparation, A.P.-G., D.J.-V. and J.A.M.-V.; writing—review and editing, J.M.E.-A. and J.C.H.-G. visualization, T.L.-H., J.D.F.-R. and J.M.E.-A. All authors have read and agreed to the published version of the manuscript.

Funding: This work was supported by CONAHCYT through the project A1-S-33363 CB/2017-2018, and "Investigadoras e investigadores por Mexico" programs (project 3155), and CF-2023-G-109. Also was supported by the University of Guanajuato "Convocatoria Institucional de Investigación Científica 2023", project CIIC 166/2023.

Institutional Review Board Statement: Not applicable.

Informed Consent Statement: Not applicable.

Data Availability Statement: The data presented in this study are available on suitable request from the corresponding author. The data are not publicly available due to privacy.

Conflicts of Interest: The authors declare no conflict of interest.

References

1. Zhu, J.J.; Zhang, A.P.; Xia, T.H.; He, S.; Xue, W. Fiber-optic high-temperature sensor based on thin-core fiber modal interferometer. *IEEE Sens. J.* **2010**, *10*, 1415–1418.
2. Díaz-Lucas, S.; San-Fabian, N.; Socorro-Leranoz, A.B.; Matias, I.R. Temperature sensor using a multiwavelength erbium-doped fiber ring laser. *Hindawi J. Sens.* **2017**, *2017*, 8187451.
3. Zhou, Y.; Zhou, W.; Chan, C.C.; Wong, W.C.; Shao, L.-Y.; Cheng, J.; Dong, X. Simultaneous measurement of curvature and temperature based on PCF-based interferometer and fiber Bragg grating. *Opt. Commun.* **2011**, *284*, 5669–5672. [CrossRef]
4. Pei, L.; Liu, C.; Li, J.; Zheng, J.; Yu, S.; Wu, L. Highly sensitive axial strain fiber laser sensor based on all-fiber acousto-optic tunable filter. *IEEE Photonics Technol. Lett.* **2014**, *26*, 2430–2433. [CrossRef]
5. Liu, Z.; Zhang, X.; Gong, Z.; Zhang, Y.; Peng, W. Fiber ring laser-based displacement sensor. *IEEE Photonics Technol. Lett.* **2016**, *28*, 1723–1726. [CrossRef]
6. Cheng, X.; Bonefacino, J.; Guan, B.O.; Tam, H.Y. All-polymer fiber-optic pH sensor. *Opt. Express* **2018**, *26*, 14610–14616. [CrossRef] [PubMed]
7. Kronenberg, P.; Rastogi, P.K.; Giaccari, P.; Limberger, H.G. Relative humidity sensor with optical fiber Bragg gratings. *Opt. Lett.* **2002**, *27*, 1385–1387. [CrossRef] [PubMed]
8. Town, G.E.; Yuan, W.; McCosker, R.; Bang, O. Microstructured optical fiber refractive index sensor. *Opt. Lett.* **2010**, *35*, 856–858. [CrossRef] [PubMed]
9. Berthold, J.W. Historical review of microbend fiber-optic sensors. *J. Light. Technol.* **1995**, *13*, 1193–1199. [CrossRef]
10. Dong, X.; Liu, Y.; Liu, Z.; Dong, X. Simultaneous displacement and temperature measurement with cantilever-based fiber Bragg grating sensor. *Opt. Commun.* **2001**, *192*, 213–217. [CrossRef]
11. Wu, C.; Fu, H.Y.; Qureshi, K.K.; Guan, B.O.; Tam, H.Y. High-pressure and high-temperature characteristics of a Fabry–Perot interferometer based on photonic crystal fiber. *Opt. Lett.* **2011**, *36*, 412–414. [CrossRef] [PubMed]
12. Jin, L.; Guan, B.O.; Wei, H. Sensitivity characteristics of Fabry-Perot pressure sensors based on hollow-core microstructured fibers. *J. Light. Technol.* **2013**, *31*, 2526–2532.
13. Yu, Q.; Zhou, X. Pressure sensor based on the fiber-optic extrinsic Fabry-Perot interferometer. *Photonic Sens.* **2011**, *1*, 72–83. [CrossRef]
14. Zhu, Y.; Wang, A. Miniature fiber-optic pressure sensor. *IEEE Photonics Technol. Lett.* **2005**, *17*, 447–449.

15. Bock, W.J.; Chen, J.; Mikulic, P.; Eftimov, T. A novel fiber-optic tapered long-period grating sensor for pressure monitoring. *IEEE Trans. Instrum. Meas.* **2007**, *56*, 1176–1180. [CrossRef]
16. Vitoria, I.; Zamarreño, C.R.; Ozcariz, A.; Matias, I.R. Fiber optic gas sensors based on lossy mode resonances and sensing materials used therefor: A comprehensive review. *Sensors* **2021**, *21*, 731. [CrossRef]
17. Zhou, J.; Liao, C.; Wang, Y.; Yin, G.; Zhong, X.; Yang, K.; Sun, B.; Wang, G.; Li, Z. Simultaneous measurement of strain and temperature by employing fiber Mach-Zehnder interferometer. *Opt. Express* **2014**, *22*, 1680–1686. [CrossRef]
18. Liao, C.R.; Wang, D.N.; Wang, Y. Microfiber in-line Mach–Zehnder interferometer for strain sensing. *Opt. Lett.* **2013**, *38*, 757–759. [CrossRef]
19. Jiang, L.; Yang, J.; Wang, S.; Li, B.; Wang, M. Fiber Mach–Zehnder interferometer based on microcavities for high-temperature sensing with high sensitivity. *Opt. Lett.* **2011**, *36*, 3753–3755. [CrossRef]
20. Socorro, A.B.; Del Villar, I.; Corres, J.M.; Arregui, F.J.; Matias, I.R. Mode transition in complex refractive index coated single-mode–multimode–single-mode structure. *Opt. Express* **2013**, *21*, 12668–12682. [CrossRef]
21. Liu, Y.; Wei, L. Low-cost high-sensitivity strain and temperature sensing using graded-index multimode fibers. *Appl. Opt.* **2007**, *46*, 2516–2519. [CrossRef] [PubMed]
22. Tripathi, S.M.; Kumar, A.; Varshney, R.K.; Kumar, Y.B.P.; Marin, E.; Meunier, J.-P. Strain and temperature sensing characteristics of single-mode–multimode–single-mode structures. *J. Light. Technol.* **2009**, *27*, 2348–2356. [CrossRef]
23. Gong, Y.; Zhao, T.; Rao, Y.J.; Wu, Y. All-fiber curvature sensor based on multimode interference. *IEEE Photonics Technol. Lett.* **2011**, *23*, 679–681. [CrossRef]
24. Wang, K.; Dong, X.; Kohler, M.H.; Kienle, P.; Bian, Q.; Jakobi, M.; Koch, A.W. Advances in optical fiber sensors based on multimode interference (MMI): A review. *IEEE Sens. J.* **2020**, *21*, 132–142. [CrossRef]
25. Yin, B.; Wang, M.; Wu, S.; Tang, Y.; Feng, S.; Wu, Y.; Zhang, H. Fiber ring laser based on MM, F-PMFBG-MMF filter for three parameters sensing. *Opt. Express* **2017**, *25*, 30946–30955. [CrossRef] [PubMed]
26. Tian, Z.; Yam, S.S.H.; Loock, H.-P. Single-mode fiber refractive index sensor based on core-offset attenuators. *IEEE Photonics Technol. Lett.* **2008**, *20*, 1387–1389. [CrossRef]
27. Yang, J.; Jiang, L.; Wang, S.; Li, B.; Wang, M.; Xiao, H.; Lu, Y.; Tsai, H. High sensitivity of taper-based Mach–Zehnder interferometer embedded in a thinned optical fiber for refractive index sensing. *Appl. Opt.* **2011**, *50*, 5503–5507. [CrossRef] [PubMed]
28. Mao, C.; Huang, B.; Huang, Y.; Zhang, L.; Shao, Y.; Wang, Y. High-sensitivity gas pressure sensor based on hollow-core photonic bandgap fiber Mach-Zehnder interferometer. *Opt. Express* **2018**, *26*, 30108–30115. [CrossRef]
29. Li, Z.; Liao, C.; Wang, Y.; Xu, L.; Wang, D.; Dong, X.; Liu, S.; Wang, Q.; Yang, K.; Zhou, J. Highly-sensitive gas pressure sensor using twin-core fiber based in-line Mach-Zehnder interferometer. *Opt. Express* **2015**, *23*, 6673–6678. [CrossRef]
30. Sun, M.; Xu, B.; Dong, X.; Li, Y. Optical fiber strain and temperature sensor based on an in-line Mach–Zehnder interferometer using thin-core fiber. *Opt. Commun.* **2012**, *285*, 3721–3725. [CrossRef]
31. Xu, B.; Li, J.; Li, Y.; Xie, J.; Dong, X. Ultrasensitive temperature sensor based on refractive index liquid-sealed thin-core fiber modal interferometers. *IEEE Sens. J.* **2013**, *14*, 1179–1184. [CrossRef]
32. Fu, H.; Zhao, N.; Shao, M.; Li, H.; Gao, H.; Liu, Q.; Yong, Z.; Liu, Y.; Qiao, X. High-sensitivity Mach–Zehnder interferometric curvature fiber sensor based on thin-core fiber. *IEEE Sens. J.* **2014**, *15*, 520–525.
33. Martin-Vela, J.A.; Sierra-Hernandez, J.M.; Jauregui-Vazquez, D.; Estudillo-Ayala, J.M.; Hernandez-Garcia, J.C.; Reyes-Ayona, J.R.; Garcia-Mina, D.F.; Rojas-Laguna, R. Highly sensitive fiber ring laser sensor for curvature using a modal interferometer. *IEEE Sens. J.* **2020**, *20*, 9864–9870. [CrossRef]
34. Xia, H.T.; Zhang, A.P.; Gu, B.; Zhu, J.J. Fiber-optic refractive-index sensors based on transmissive and reflective thin-core fiber modal interferometers. *Opt. Commun.* **2010**, *283*, 2136–2139. [CrossRef]
35. Liu, Y.; Lin, H.; Dai, Y.; Zhou, A.; Yuan, L. Fiber in-line Mach–Zehnder interferometer for gas pressure sensing. *IEEE Sens. J.* **2018**, *18*, 8012–8016. [CrossRef]
36. Xu, B.; Li, J.Q.; Li, Y.; Dong, X.Y. A thin-core fiber modal interferometer for liquid-level sensing. *Chin. Phys. Lett.* **2012**, *29*, 104209. [CrossRef]
37. Gu, B.; Yin, M.J.; Zhang, A.P.; Qian, J.W.; He, S. Low-cost high-performance fiber-optic pH sensor based on thin-core fiber modal interferometer. *Opt. Express* **2009**, *17*, 22296–22302. [CrossRef]
38. Wu, Q.; Semenova, Y.; Mathew, J.; Wang, P.; Farrell, G. Humidity sensor based on a single-mode hetero-core fiber structure. *Opt. Lett.* **2011**, *36*, 1752–1754. [CrossRef]
39. Huang, X.; Li, X.; Yang, J.; Tao, C.; Guo, X.; Bao, H.; Yin, Y.; Chen, H.; Zhu, Y. An in-line Mach-Zehnder interferometer using thin-core fiber for ammonia gas sensing with high sensitivity. *Sci. Rep.* **2017**, *7*, 44994. [CrossRef]
40. Zhao, Y.; Li, H.; Li, J.; Zhou, A. Cascaded fiber MZIs for simultaneous measurement of pressure and temperature. *Opt. Fiber Technol.* **2021**, *66*, 102629. [CrossRef]
41. Zhao, Y.; Cai, I.; Li, X.-G. In-Fiber Mach-Zehnder Interferometer Based on Up-Taper Fiber Structure with Er^{3+} Doped Fiber Ring Laser. *J. Light. Technol.* **2016**, *34*, 3475–3481. [CrossRef]
42. Xie, W.-G.; Zhang, Y.-N.; Wang, P.-Z.; Wang, J.-Z. Optical Fiber Sensors Based on Fiber Ring Laser Demodulation. *Technol. Sens.* **2018**, *18*, 505. [CrossRef]
43. Contreras, M.A. Temperature Sensor Using Fiber Ring Laser Based On a Core-Offset Mach-Zehnder Interferometer. *Supl. Rev. Mex. Fis.* **2021**, *2*, 109–115. [CrossRef]

44. Jasim, A.A.; Ahmad, H. A highly stable and switchable dual-wavelength laser using coupled microfiber Mach-Zehnder interferometer as an optical filter. *Opt. Laser Technol.* **2017**, *97*, 12–19. [CrossRef]
45. Shi, J.; Wang, Y.; Xu, D.; He, Y.; Jiang, J.; Xu, W.; Zhang, H.; Su, G.; Yan, C.; Yan, D.; et al. Remote gas pressure sensor based on fiber ring laser embedded with Fabry–Perot interferometer and sagnac loop. *IEEE Photonics J.* **2016**, *8*, 1–8. [CrossRef]
46. Yin, Z.; Gao, L.; Liu, S.; Zhang, L.; Wu, F.; Chen, L.; Chen, X. Fiber ring laser sensor for temperature measurement. *J. Light. Technol.* **2010**, *28*, 3403–3408.
47. Zhao, Z.Q.; Lu, Y.; Duan, L.C.; Wang, M.T.; Zhang, H.W.; Yao, J.Q. Fiber ring laser sensor based on hollow-core photonic crystal fiber. *Opt. Commun.* **2015**, *350*, 296–300. [CrossRef]
48. Yamashita, S.; Hotate, K. Distributed pressure sensor with a mode-locked fiber-ring laser. *Opt. Lett.* **2001**, *26*, 590–592. [CrossRef]
49. Talataisong, W.; Wang, D.N.; Chitaree, R.; Liao, C.R.; Wang, C. Fiber in-line Mach-Zehnder interferometer based on an inner air-cavity for high-pressure sensing. *Opt. Lett.* **2015**, *40*, 1220–1222. [CrossRef]

Disclaimer/Publisher's Note: The statements, opinions and data contained in all publications are solely those of the individual author(s) and contributor(s) and not of MDPI and/or the editor(s). MDPI and/or the editor(s) disclaim responsibility for any injury to people or property resulting from any ideas, methods, instructions or products referred to in the content.